The Effect of Pipe-Wall Boundary Layer Thickness on the Shape of Taylor Bubbles in Vertical pipes

Boonchai Lertnuwat
Dept. of Mechanical Engineering, Faculty of Engineering,
Chulalongkorn University, Phayathai Rd., Pathum Wan, Bangkok 10330, Thailand

Abstract

The shape of Taylor bubbles in slug flow relates to the flow in a narrow falling film, which is highly affected on the pipe-wall boundary layer. In this work, the boundary layer thickness is taken into account for deriving a model predicting the shape of a Taylor bubble. The result of the present model will be compared to the result of previous models, which do not take into accunt the effect of boundary layer thickness. This comparison will reveal more insight about the effect of boundary layer thickness on Taylor bubble shape in vertical pipelines. Finally, it shows that the present model can comparatively predict the shape of Taylor bubbles for bubble heads, but much better for bubble tails. The improper shape of bubble heads results from the assumption that boundary layer thickness starts to develop at bubble noses. However, this is still acceptable and the present model is conclusively good for predicting the shape of Taylor bubbles.

Keywords: Slug flow, Taylor bubble, Boundary Layer and Kinematic energy coefficient

2. Nomenclatures

2.1 Characters

D	Pipe diameter
g	Gravity acceleration
$\dot{m}$	Mass flow rate
p	Static pressure
R	Distance of interface referred to r-axis
r	Distance referred to r-axis
u	Velocity component on z-axis
V	Total velocity
v	Velocity component on r-axis
y	Distance from pipe wall
z	Distance referred to z-axis

2.2 Symbols

α	Kinematic energy coefficient
χ	$[(D/2)-R]/\delta$
δ	Boundary layer thickness
ρ	Density

2.3 Superscripts and Subscripts

0	Location at bubble nose
$D\&T$	Dumitresku & Taylor model
d	Drift
∞	Infinity
l	Liquid
m	Mixture
tr	Translation

3. Introduction

Taylor bubbles are known as elongation bubbles drifting in slug flow. In vertical pipes, Taylor bubbles tend to have axis-symmetric shape along centerlines of the pipes. The shape of a Taylor bubble affects the pressure of flow in the falling film region around the bubble by the change of a dynamic pressure. Generally, static pressure in falling film is assumed to be constant and equal to the gas pressure inside the Taylor bubble in the case that tension effects are neglected. The assumption of constant pressure is widely used in many works. Barnea [1] who demonstrated that this assumption for flat nosed Taylor bubble leads to wrong pressure drop across a slug unit, explained that gas in the Taylor bubble is at a constant pressure since the gas density and viscosity are much lower than the liquid density and viscosity. This results in negligible interfacial shear and the liquid film is assumed to flow around the Taylor bubble as a free falling film. Bugg *et al.* [2] composed a computational algorithm for investigating the shape of a Taylor bubble by using a void

fraction specification to track the movement of the gas-liquid interface. In this work, the pressure difference within a gas-filled control volume is set to be zero, indicating constant pressure in any bubbles present in the flow field. Clarke and Issa [5] numerically predict Taylor bubble shape by employing $k-\varepsilon$ model and moving grid technique. They claimed that experiment showed that the pressure drop over the Taylor bubble is zero. This is the reason why they set a certain physical condition of constant pressure inside the Taylor bubble in order to determine the shape of the bubble. Also, Mao and Dukler [10] tried to determine Taylor bubble shape by using Navier-Strokes equation and staggered grid system, which is designed to intersect at the gas-liquid interface. The staggered grid system moves along the change of interface curvature to maintain pressure inside Taylor bubble to be constant. The writers stated that experimental data confirmed this. Hence, the shape of a Taylor bubble is very important for governing the flow field around it to maintain constant static pressure. This is the reason why the shape of Taylor bubbles has been studied so much.

Nigmatulin and Bonetto [12] gave background about the shape of Taylor bubbles having a length more than $5D$ of pipe. They stated that such long bubbles could be divided into 3 regions, whose shape can be respectively predicted by

Dumitresku model:

$$R=\frac{D}{2}-\frac{1}{2}\sqrt{z(3d-4z)} \quad (1)$$

Taylor model: $$R=\frac{D}{2}\sqrt{1-\frac{u_{tr}}{\sqrt{2gz}}} \quad (2)$$

Nusselt model: $$R=const \quad (3)$$

They also have done experiments on single Taylor bubbles in 15.6 mm-dia. pipe. The shape of Taylor bubbles predicted by the series of models was compared with experimental results. It is found that the models overestimated the size of Taylor bubbles in comparison to the experimental results. The discrepancy between models' result and experimental result is also confirmed by Mao and Dukler [11]. They used their own numerical simulation for predicting Taylor bubble shape to compare the simulated results with experimental results and the results calculated by Dumitresku model. They have found that the Dumitresku model gave the largest bubble size, whereas experiment gave the smallest bubble size. Their numerical simulation gave results in between both former results. This is quite unclear under low Re conditions but much more obvious at high Re of fluid flow. Clarke and Issa [5] had compared their computational results of bubble shape to experimental results of Mao and Dukler [11] and the results calculated by the Dumetresku model. The comparison showed that, in stagnant fluid, the shape of bubble predicted by their computational simulation agrees well with that predicted by the Dumetresku model but is larger than the results from experiment.

Some important factors are possibly not considered in the former models. The gas-liquid interface is believed to be free-shear, whereas the pipe wall is practically assumed to be governed by no-slip conditions, leading to the presence of boundary layers. In large pipes, the boundary layer is likely not to disturb the flow field in the pipe seriously. Contrary to small pipes, flow in the pipes is violently disturbed by the boundary layer when the boundary layer thickness (δ) has the same order of magnitude of the pipe diameter. This is similar to the flow field in the falling film region, when the hydraulic pipe diameter is close to the boundary layer thickness. In this work, the boundary layer thickness is taken into account for deriving a model predicting the shape of Taylor bubbles. The result of the present model will be compared to the results of previous models to gain insight about the effect of boundary layer thickness on Taylor bubble shape in vertical pipelines.

4. Modeling

The energy equation of fluid flow is exploited as the fundamental equation for predicting the shape of Taylor bubbles in vertical pipe.

$$p_0+\frac{1}{2}\alpha_0\rho_m\bar{V}_0^2-\rho_m g z_0 = p+\frac{1}{2}\alpha\rho_m\bar{V}^2-\rho_m g z \quad (4)$$

The negative sign in front of variable z implies the depth measured along the z-axis as shown in

Fig.1. The second term on both sides of eq.(4) is the dynamic pressure calculated by average total velocity at any considered point. Since the direction of flow velocity in the falling film region is almost parallel to the pipe centerline, it is, thus, reasonable to substitute the z-component of velocity into total velocity. This yields:

$$p_0 + \frac{1}{2}\alpha_0 \rho_m \bar{u}_0^2 - \rho_m g z_0 = p + \frac{1}{2}\alpha \rho_m \bar{u}^2 - \rho_m g z \qquad (5)$$

The influence of pipe-wall boundary layer is involved through the kinetic energy coefficient α, which is generally defined as follows:

$$\alpha = \left[\int_A \rho_m u^3 dA\right] \Big/ \left(\dot{m}\bar{u}^2\right) = \left[2\int_R^{D/2} \left(u^3 r\right) dr\right] \Big/ \left[\left(\frac{D^2}{4} - R^2\right)\bar{u}^3\right] \qquad (6)$$

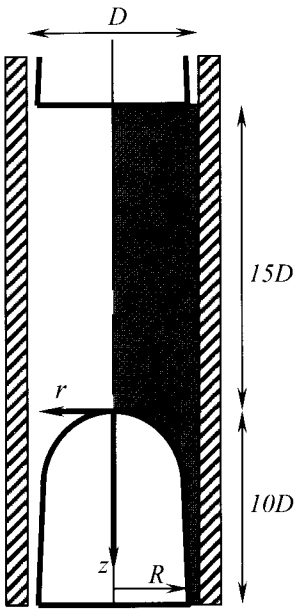

Figure 1: The schematic diagram of the computation domain, confined in the shaded area.

According to Eq.(6) the profile of fluid velocity is necessary for defining the value of α at any cross-section. To achieve this, the flow condition in the falling film is to be specified whether it is laminar or turbulent. From their experiments of Taylor bubbles rising in stagnant liquid, Mao and Dukler [11] had concluded that the falling film had experienced laminar-to-turbulence transition when the pipe-wall boundary layer had developed near a certain Re, leading to a wavy interface at the bottom of the bubble. This is confirmed by Clarke and Issa [5]. After they had compared their computational result of wall shear stress to the experimental results of Mao and Dukler [11], they found that their computational outcome agreed well with the experimental reference just within 300 mm behind the bubble nose in a 0.05 m-dia. pipe. Although they explained that the discrepancy is caused by laminar-to-turbulence transition owning to the nature of wavy interface, their computation was carried out on the assumption that the flow remains laminar throughout the thin film and the their computational results came out reasonable. Consequently, in this work, the velocity profile is assumed to be laminar-like parabolic and written as below:

$$u = \begin{cases} u_{tr} + 2\dfrac{\left(u_\infty - u_{tr}\right)}{\delta} y - \dfrac{\left(u_\infty - u_{tr}\right)}{\delta^2} y^2 & ; y < \delta \\ u_\infty & ; y \geq \delta \end{cases} \qquad (7)$$

Since the relation between y and r is known as:

$$y = \frac{D}{2} - r \qquad (8)$$

eq.(7) will be rewritten so that r is explicitly shown as follow:

$$u = \begin{cases} u_{tr} + 2\dfrac{\left(u_\infty - u_{tr}\right)}{\delta}\left(\dfrac{D}{2} - r\right) - \dfrac{\left(u_\infty - u_{tr}\right)}{\delta^2}\left(\dfrac{D}{2} - r\right)^2 & ; y < \delta \\ u_\infty & ; y \geq \delta \end{cases} \qquad (9)$$

By substituting eq.(9) into eq.(6) and assuming that $\delta >> D$, we obtain:

$$\alpha = \frac{u_\infty^3}{\overline{u}^3} - \left[\frac{1}{35}(u_\infty - u_{tr})(19u_\infty^2 + 11u_\infty u_{tr} + 5u_{tr}^2)(\delta D)\right] \Big/ \left[\left(\frac{D^2}{4} - R^2\right)\overline{u}^3\right] \quad (10)$$

Focusing on the second term of eq.(10), there are 2 interesting points. First, this term will be small around bubble noses since $u_\infty \approx u_{tr}$. Second, u_{tr} can be neglected in the region close to the bubble bottom where $u_\infty >> u_{tr}$. Therefore the second term on the right-hand-side of eq.(10) can be reduced and eq.(10) becomes:

$$\alpha = \frac{u_\infty^3}{\overline{u}^3}\left[1 - \frac{19}{35}\frac{(\delta D)}{\left(\frac{D^2}{4} - R^2\right)}\right] \quad (11)$$

Eq.(11) still has 2 unknown variables, i.e. velocity ratio ($u_\infty/\overline{u}$) and boundary layer thickness (δ), which are respectively determined.

The velocity ratio between free-stream velocity and average velocity at any cross-sectional area is defined as:

$$\frac{\overline{u}}{u_\infty} = \left[\int_A u dA\right] \Big/ (Au_\infty) = \left[2\int_R^{D/2}(ur)dr\right] \Big/ \left[\left(\frac{D^2}{4} - R^2\right)u_\infty\right] \quad (12)$$

Identical to the case of deriving Kinematic energy coefficients, the velocity profile is assumed to be parabolic as already shown in eq.(9). Substituting eq.(9) into eq.(12) and assuming that $\delta >> D$ yields:

$$\frac{\overline{u}}{u_\infty} = 1 - \frac{1}{3}\left(1 - \frac{u_{tr}}{u_\infty}\right)\delta D \Big/ \left(\frac{D^2}{4} - R^2\right) \quad (13)$$

The translational velocity on the right-hand-side of eq.(13) can be related to the average velocity at any cross-sectional area in the falling film by employing continuity equation under steady state condition as:

$$\rho_{m0}u_{tr}\left(\frac{D^2}{4}\right) = \overline{\rho}_m\overline{u}\left(\frac{D^2}{4} - R^2\right)$$

Mixture density is a function of dispersed bubble distribution, which has many patterns, e.g. core-peak distribution and wall-peak distribution, depending on several factors. Nevertheless some researchers still use uniform bubble distribution in their works. For instance, Mao and Dukler [9] who have explained the different terminal velocity between a train of Taylor bubbles and a single Taylor bubble, exploited cross-sectional average velocity of the dispersed bubble in liquid slug in their calculation, inferring a uniform distribution of the dispersed phase. This is also found in the work of Clarke and Issa [5]. Although realizing that the dispersed phase in a slug is distributed unevenly across the pipe sectional area, they assumed a homogeneous gas-liquid mixture in the liquid slug as a first-order approximation in their numerical model for studying Taylor bubble shape. Moreover, it is naturally found that the dispersed bubbles merge to the nose of Taylor bubbles and re-entrain from the tail of bubbles. Consequently, when flow in falling film is considered, the density of mixture in slug flow is assumed to distribute uniformly with value close to liquid density, resulting in:

$$u_{tr} = \overline{u}\left(\frac{D^2}{4} - R^2\right) \Big/ \left(\frac{D^2}{4}\right) \quad (14)$$

Substituting eq.(14) into eq.(13) and assuming that $\delta >> D$, we obtain:

$$\frac{\overline{u}}{u_\infty} = \left(\frac{D^2}{4} - R^2 - \frac{\delta D}{3}\right) \Big/ \left(\frac{D^2}{4} - R^2\right) \quad (15)$$

It is valuable to note that the term $\left(\frac{D^2}{4} - R^2 - \frac{\delta D}{3}\right)$ cannot be reduced since it is:

a) close to Taylor bubble nose ($R \approx 0$), the order of magnitude of :

$$\frac{D^2}{4} - R^2 \approx \frac{D^2}{4} - 0 = \frac{D^2}{4} >> \delta D \quad (16)$$

b) close to Taylor bubble bottom ($R \approx D/2$), the order of magnitude of :

$$\frac{D^2}{4} - R^2 = \left(\frac{D}{2} - R\right)\left(\frac{D}{2} + R\right) \approx \delta D \quad (17)$$

Therefore, δD cannot be neglected from these parentheses in the falling film region. Finally eq.(15) is rewritten in more applicable format as:

$$\left(\frac{u_\infty}{\bar{u}}\right)^3 = \left(\frac{D^2}{4} - R^2\right)^3 \Bigg/ \left(\frac{D^2}{4} - R^2 - \frac{\delta D}{3}\right)^3$$
$$= \left(\frac{D^2}{4} - R^2\right)^3 \Bigg/ \left[\left(\frac{D^2}{4} - R^2\right)^3 - \left(\frac{D^2}{4} - R^2\right)^2 (\delta D) + \frac{1}{3}\left(\frac{D^2}{4} - R^2\right)(\delta D)^2 - \frac{1}{27}(\delta D)^3\right] \quad (18)$$

In accordance with eq.(16) and eq.(17), the last term in the denominator of the quotient on the right-hand-side of eq.(18) is always much less than the third term. It will be neglected and we get :

$$\left(\frac{u_\infty}{\bar{u}}\right)^3 \approx \left(\frac{D^2}{4} - R^2\right)^2 \Bigg/ \left[\left(\frac{D^2}{4} - R^2\right)^2 - \left(\frac{D^2}{4} - R^2\right)(\delta D) + \frac{1}{3}(\delta D)^2\right] \quad (19)$$

which is going to be employed in eq.(11)

The next unknown variable left in eq.(11) is the boundary layer thickness (δ). To derive δ , the momentum integral equation under steady state condition is needed. Fig.2 shows the differential control volume occupying the boundary layer, adjacent to the pipe wall. Due to the continuity equation, the mass flux across the upper boundary of the element shown in Fig.2 is :

$$\rho_{m\infty} v_\infty = -\frac{d}{dz}\left(\int_0^\delta \rho_m u\, dy\right) \quad (20)$$

Due to the momentum equation, the relation among shear force, momentum flux, pressure and gravity can be written as

$$\tau_w = u_\infty \frac{d}{dz}\left(\int_0^\delta \rho_m u dy\right) - \frac{d}{dz}\left(\int_0^\delta \rho_m u^2 dy\right) \quad (21)$$

The last term on the right-hand-side of eq.(21) will relate to free stream as:

$$\left(\rho_m g - \frac{dp}{dz}\right)\int_0^\delta dy = \left(\rho_m u_\infty \frac{du_\infty}{dz}\right)\int_0^\delta dy \quad (22)$$

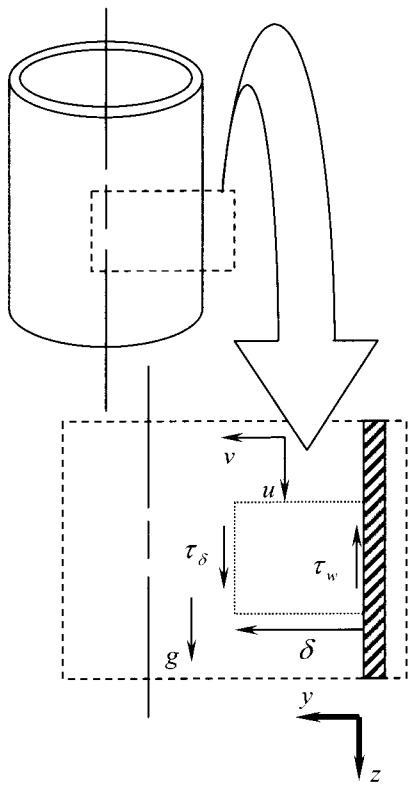

Figure 2: Differential volume element of flow adjacent to pipe wall.

Adding eq.(21) with eq.(22), we get :

$$\tau_w = u_\infty \frac{d}{dz}\left(\int_0^\delta \rho_m u dy\right) - \frac{d}{dz}\left(\int_0^\delta \rho_m u^2 dy\right) + \left(\rho_m u_\infty \frac{du_\infty}{dz}\right)\int_0^\delta dy \quad (23)$$

As previous, the density of mixture in slug flow is assumed to be uniform, eq.(23) becomes eq.(24) with simple manipulation:

$$\frac{\tau_w}{\rho_m} = \frac{d}{dz}\left[\int_0^\delta u(u_\infty - u)dy\right] + \frac{du_\infty}{dz}\left[\int_0^\delta (u_\infty - u)dy\right]$$

$$\nu\frac{du}{dy} = \frac{d}{dz}\left[\int_0^\delta u(u_\infty - u)dy\right] + \frac{du_\infty}{dz}\left[\int_0^\delta (u_\infty - u)dy\right] \quad (24)$$

Exploiting velocity profile stated in eq.(9), after integrating, eq.(24) becomes:

$$30\nu\frac{(u_\infty - u_{tr})}{\delta} = \frac{d}{dz}\left[\left(2u_\infty^2 + u_\infty u_{tr} - 3u_{tr}^2\right)\delta\right] + 25(u_\infty - u_{tr})\delta\frac{du_\infty}{dz}$$

$$30\nu(u_\infty - u_{tr}) = \delta\frac{d}{dz}\left[\left(2u_\infty^2 + u_\infty u_{tr} - 3u_{tr}^2\right)\delta\right] + 25(u_\infty - u_{tr})\delta^2\frac{du_\infty}{dz} \quad (25)$$

Let us consider the product $(u_\infty - u_{tr})\delta$. This term can be approximately reduced to be $u_\infty\delta$ because:

Close to Taylor bubble nose, $\delta \approx 0$, so

$$(u_\infty - u_{tr})\delta \approx (u_\infty - u_{tr})0 \quad \text{or}$$

$$(u_\infty)0 = 0 \approx (u_\infty)\delta \quad (26)$$

Close to Taylor bubble bottom, $u_\infty >> u_{tr}$, so

$$(u_\infty - u_{tr})\delta \approx (u_\infty)\delta \quad (27)$$

Similar to the product $\left(2u_\infty^2 + u_\infty u_{tr} - 3u_{tr}^2\right)\delta$, it can be approximated as $2u_\infty^2\delta$ for the same reason. As a result, eq.(25) will turn out to be:

$$30\nu(u_\infty - u_{tr}) = \delta\frac{d}{dz}\left[2u_\infty^2\delta\right] + 25u_\infty\delta^2\frac{du_\infty}{dz}$$

$$30\nu(u_\infty - u_{tr}) = 2u_\infty^2\delta\frac{d\delta}{dz} + 29\delta^2 u_\infty\frac{du_\infty}{dz} \quad (28)$$

Reviewing eq.(22), the equation relates pressure gradient to gravity and free stream velocity. In the case that this equation is applied to flow in a falling film, the pressure gradient term will be zero due to the constraint that pressure on the bubble interface is constant as already demonstrated in the introduction section. By forcing pressure to be constant in the falling film region, eq.(22), thus, becomes:

$$g = u_\infty\frac{du_\infty}{dz} \quad (29)$$

$$u_\infty^2 = u_{tr}^2 + 2gz \quad (30)$$

Substituting eq.(29) and eq.(30) into eq.(28), we obtain:

$$30\nu\left(\sqrt{u_{tr}^2 + 2gz} - u_{tr}\right) = 2\left(u_{tr}^2 + 2gz\right)\delta\frac{d\delta}{dz} + 29g\delta^2 \quad (31)$$

The term $\left(u_{tr}^2 + 2gz\right)\delta$ can be reduced to be $2gz\delta$. This is because $u_{tr}^2 << 2gz$ when z is larger. And this term approaches zero due to the value of δ when z is small. Applying this approximation to eq.(31) results in:

$$30\nu\left(\sqrt{u_{tr}^2 + 2gz} - u_{tr}\right) = 4gz\delta\frac{d\delta}{dz} + 29g\delta^2 \quad (32)$$

The term $\sqrt{u_{tr}^2 + 2gz}$ in eq.(32) can be approximated by Taylor series, $f(x + \Delta x) = f(x) + \Delta x f'(x)$. However, the problem is that there are 2 choices, i.e.

a) We choose $x = u_{tr}^2$ and $\Delta x = 2gz$.

b) We choose $x = 2gz$ and $\Delta x = u_{tr}^2$.

The accuracy of Taylor series depends on the size of Δx, or comparatively the ratio of $\Delta x / x$. Here we have found that choice (b) is better when z is large but gives comparatively more error when $\Delta x / x = u_{tr}^2 / 2gz >> 1$. In the case that a Taylor bubble drifts freely in the pipeline, we have $u_{tr}^2 = u_d^2 = (0.345)^2 gD$. This means that the choice (b) gives more error when $u_{tr}^2 / 2gz = 0.06D / z >> 1$ or $z << 0.06D$, which is very narrow region close to bubble nose. Hence, choice (b) is better for approximating that :

$$\sqrt{u_{tr}^2 + 2gz} = \sqrt{2gz} + u_{tr}^2\left[d\sqrt{2gz} / d(2gz)\right]$$

$$= \sqrt{2gz} + u_{tr}^2 / \sqrt{8gz} \quad (33)$$

Substituting eq.(33) into eq.(32), we get :

$$30\nu\left[\sqrt{2gz} - \left(1 - u_{tr}/\sqrt{8gz}\right)u_{tr}\right] = 4gz\delta\frac{d\delta}{dz} + 29g\delta^2 \quad (34)$$

which can be approximated as eq.(35) with acceptable error in the region close to bubble nose (approximately $z << 0.06D$ as stated previously).

$$30\nu\sqrt{2gz} = 4gz\delta\frac{d\delta}{dz} + 29g\delta^2$$

$$\frac{1}{2}\frac{d\delta^2}{dz} = \frac{15\nu}{\sqrt{2gz}} - \frac{29\delta^2}{4z} \quad (35)$$

To solve eq.(35), we let :

$$\xi = \delta^2 \quad (36)$$

$$\beta^2 = z \quad (37)$$

then eq.(35) becomes:

$$\frac{d\xi}{d\beta} = \frac{60\nu}{\sqrt{2g}} - 29\frac{\xi}{\beta} \quad (38)$$

It is obvious that eq.(38) is a homogeneous equation, which can be solved by assign that:

$$\xi = \Psi\beta \quad (39)$$

$$\frac{d\xi}{d\beta} = \Psi + \beta\frac{d\Psi}{d\beta} \quad (40)$$

Substituting eq.(39) and eq.(40) into eq.(38), we obtain:

$$\beta\frac{d\Psi}{d\beta} = \frac{60\nu}{\sqrt{2g}} - 30\Psi \quad (41)$$

which after being integrated yields:

$$\Psi = \left[\nu\sqrt{\frac{2}{g}} - c\beta^{-30}\right] \quad (42)$$

in which c is any constant. Next, by applying eq.(39), eq.(37) and eq.(36), we obtain:

$$\delta = \left[\nu\sqrt{\frac{2z}{g}} - cz^{-\frac{29}{2}}\right]^{\frac{1}{2}} \quad (43)$$

The constant c is set to be zero to make eq.(43) finite at $z = 0$. Hence, we eventually obtain the equation for predicting boundary layer thickness as:

$$\delta = \left[\nu\sqrt{\frac{2z}{g}}\right]^{\frac{1}{2}} \quad (44)$$

which explicitly shows that the boundary layer thickness in the falling film region develops with $z^{0.25}$

For all necessary equations ($u_\infty/\bar{u}$ and δ), for substituting in eq.(11), Kinetic energy coefficients are obtained. The next step, eq.(5) is recalled and re-arranged to get dynamic pressure explicitly exhibited.

$$\frac{1}{2}\alpha_0\rho_m\bar{u}_0^2 - \frac{1}{2}\alpha\rho_m\bar{u}^2 = p - p_0 + \rho_m g z_0 - \rho_m g z \quad (45)$$

By assuming that static pressure in the falling film region is constant and mixture density is uniform, which are respectively consistent with eq.(29) and eq.(14), eq.(45) reduces to be:

$$\alpha\bar{u}^2 - \alpha_0\bar{u}_0^2 = 2g(z - z_0)$$

Since, at bubble noses ($z_0 = 0$), the boundary layer thickness is zero as shown in eq.(44), the velocity profile is uniformly equal to u_{tr} and the Kinematic energy coefficient is unity ($\alpha_0 = 0$). Therefore, we get :

$$\alpha\bar{u}^2 - u_{tr}^2 = 2gz \quad (46)$$

Applying eq.(11) and eq.(14), we get :

$$\left[\left(\frac{u_\infty}{\bar{u}}\right)^3\left[1 - \frac{19}{35}\frac{(4\delta D)}{(D^2 - 4R^2)}\right]\left(\frac{D^2}{D^2 - 4R^2}\right)^2 - 1\right]u_{tr}^2 = 2gz$$

$$\left(\frac{u_\infty}{\bar{u}}\right)^3\left[1 - \frac{19}{35}\frac{(4\delta D)}{(D^2 - 4R^2)}\right]\left(\frac{D^2}{D^2 - 4R^2}\right)^2 = 1 - \frac{2gz}{u_{tr}^2} \quad (47)$$

Substituting eq.(19) into eq.(47), we get :

$$\lambda^3+\left(-4\frac{\delta}{D}\right)\lambda^2+\left[\frac{16}{3}\left(\frac{\delta}{D}\right)^2-\gamma\right]\lambda+\frac{76}{35}\gamma\left(\frac{\delta}{D}\right)=0 \quad (48)$$

Herein, new variables are defined as follows:

$$\lambda=\left(D^2-4R^2\right)/D^2 \quad (49)$$

$$\gamma=\left(1+\frac{2gz}{u_{tr}^2}\right)^{-1} \quad (50)$$

In the case that boundary layer thickness is not considered, eq.(48) will yield the model proposed by Barnea [1] which neglects shear stress. However, when the boundary layer thickness is involved, eq.(48) becomes a cubic equation, which can be solved by re-writing in simpler form as:

$$\lambda^3+a\lambda^2+b\lambda+c=0 \quad (51)$$

Next, let:

$$\lambda'=\lambda-a/3 \quad (52)$$

we obtain:

$$\lambda'^3=\left(\frac{1}{3}a^2-b\right)\lambda'+\left(\frac{ab}{3}-\frac{2}{27}a^3-c\right) \quad (53)$$

which can be solved by assigning that :

$$\psi=\frac{1}{3}\left(\frac{1}{3}a^2-b\right)=\frac{1}{3}\gamma \quad (54)$$

$$\zeta=\frac{1}{2}\left(\frac{ab}{3}-\frac{2}{27}a^3-c\right)=-\frac{1}{2}\left(\frac{\delta}{D}\right)\left[\frac{64}{27}\left(\frac{\delta}{D}\right)^2+\frac{88}{105}\gamma\right] \quad (55)$$

$$\zeta^2-\psi^3=\frac{1}{4}\left(\frac{64}{27}\right)^2\left(\frac{\delta}{D}\right)^6+\frac{1}{2}\left(\frac{64}{27}\right)\left(\frac{88}{105}\right)\gamma\left(\frac{\delta}{D}\right)^4+\frac{1}{4}\left(\frac{88}{105}\right)^2\gamma^2\left(\frac{\delta}{D}\right)^2-\frac{1}{27}\gamma^3 \quad (56)$$

The sign of $\zeta^2-\psi^3$ in eq.(56) is important for determining λ and it can be considered as follows. First, the magnitude of γ is approximated by using eq.(48) and assuming that $\delta << D$. Hence, we get:

$$\lambda^3-\gamma\lambda\approx 0$$

$$\gamma\approx\lambda^2=\left[\frac{D^2-4R^2}{D^2}\right]^2$$

Since $R\approx 0$ at a location close to the bubble nose and $R\approx(D/2)-\delta$ at a location close to the bubble bottom, we get the magnitude of γ as follows:

$$\gamma\approx\begin{cases}1 & ;R\approx 0\\ 16\left(\frac{\delta}{D}\right)^2 & ;R\approx\frac{D}{2}-\delta\end{cases} \quad (57)$$

This means that:

$$\zeta^2-\psi^3\approx\begin{cases}-\frac{1}{27} & ;R\approx 0\\ -80.77\left(\frac{\delta}{D}\right)^6 & ;R\approx\frac{D}{2}-\delta\end{cases} \quad (58)$$

It is clear that $\zeta^2-\psi^3$ in eq.(56) is always negative, leading to the root of eq.(53) being equal to:

$$\lambda'=2\sqrt{\psi}\cos(\phi/3) \quad (59)$$

$$\cos\phi=\zeta/\psi^{1.5}\ ;0^o\le\phi\le 180^o \quad (60)$$

Exploiting eq.(52), eq.(51) and eq.(48), we get :

$$\lambda=\lambda'+\frac{4}{3}\frac{\delta}{D} \quad (61)$$

Eventually, by applying eq.(49), we get the model to predict the shape of Taylor bubble as:

$$R=\frac{D}{2}\sqrt{1-\lambda'-\frac{4}{3}\frac{\delta}{D}} \quad (62)$$

Note that there are, in fact, 2 other roots of eq.(53). But both of them give impractical solutions for R because:

$\lambda_2' = 2\sqrt{\psi}\cos(\phi/3 + 120^o)$, always gives a negative result, and

$\lambda_3' = 2\sqrt{\psi}\cos(\phi/3 + 240^o)$, gives $R \neq 0$ at the bubble nose ($z = 0$).

5. Model Verification

The present model in the previous section is used to predict the shape of Taylor bubbles for studying the effect of boundary layer thickness by comparing with the shape of Taylor bubbles predicted by eq.(1) and eq.(2). The eq.(3) is omitted since Nigmatulin and Bonetto [12] did not give adequate information to merge this constant film thickness to the second part of the bubble although they recommended that eq.(3) should be used when the bubble is long enough that gravity in the film balances with wall shear. Another model for calculating the constant film thickness belongs to Wallis, which is referred to Barnea [1]. It is not employed in this paper because it considers the effect of shear force, which may lead us to compare two different parameters, i.e. boundary layer thickness and shear force.

Flow around Taylor bubbles predicted by all models is computed by $k-\varepsilon$ model for compressible flow, which is discretized by pressure correction scheme on finite volume framework. A cylindrical collocated grid system is used. The problem of checkerboard distribution is resolved by the technique called "Treatment of pressure". The No-slip condition along pipe wall is treated with a wall function, which relies on a logarithmic velocity profile and the equilibrium between production and dissipation of turbulent kinetic energy. The detail of numerical algorithm can be found in Ferziger and Peric [7].

By assuming that the Taylor bubble rises along the centerline of the pipe, axis-symmetric cylindrical coordinates are exploited as shown in Fig.1. The computational domain has 2 regions, i.e. liquid slug and falling film surrounding a Taylor bubble. The length of liquid slug and Taylor bubble are selected to be consistent to the dimension of slug flows found in previous works. For example, Clarke and Issa [5] composed a computational algorithm for predicting the shape of bubbles, whose length ranges from $5D$ to $23D$, with slug length ranging from $10D$ to $46D$. Mao and Dukler [11] studied interfacial shear stress on bubble surface with modified $k-\varepsilon$ model with $6.2D$-long bubble. Van Hout *et al.* [16] statically investigated the length of liquid slugs and Taylor bubbles in pipes. The average length of Taylor bubble is between $4D$ and $18.9D$ in a 54 mm pipe, depending on flowrate and the distance from the base of the testing section. They also found that slug length is about $17D$ in a 24 mm pipe. Table 1 summarizes the data obtained from previous literature. Most experiments revealed that there was a likely equilibrium size for slug length but not for Taylor bubble length, which is elongating along the altitude of the pipe. According to the information summarized in Table 1, in this work, slug length and Taylor bubble length are selected to be $15D$ and $10D$, respectively.

Table 1: Statistical Parameters of Gas-Liquid Slug Flow along Vertical Pipes

References	Pipe Dia.	Slug length	Bubble length
Clarke and Issa [5]	50 mm	*10-46D*	*5-23D*
Mao and Dukler [11]	50.8 mm		*6.2D*
Shemer [14]	24 mm	*16.3D*	
Van Hout *et al.* [16]	24 mm 54 mm	*~17D* in 24 mm pipe	*4-18.9D* in 54 mm pipe
Van Hout *et al.* [18]	24 mm	*16.3D*	*6.3-28.6D*

The diameter of pipe is an important parameter, which needs analysis for determining. According to eq.(62), it is found that the shape of a Taylor bubble is a function of λ' and δ/D. The λ' is defined by eq.(59) and eq.(60). This implies that λ' is a function of γ and δ/D, owning to eq.(54) and eq.(55). Employing eq.(50), we can find that:

$$\gamma = \left(1+\frac{2gz}{u_{tr}^2}\right)^{-1} = \left(1+\frac{2gD}{u_{tr}^2}\frac{z}{D}\right)^{-1} = \left(1+\frac{2}{Fr}\left(\frac{u_d}{u_{tr}}\right)^2\frac{z}{D}\right)^{-1} \quad (63)$$

Where, for ideal fluid with low tension ($Eo > 70$) as discussed in White and Beardmore [19]:

$$Fr = \left(u_d / \sqrt{gD}\right)^2 = 0.345^2 \qquad (64)$$

Next, employing eq.(44), we can find that :

$$\frac{\delta}{D} = \left[\frac{\nu}{D^2}\sqrt{\frac{2z}{g}}\right]^{\frac{1}{2}} = \left[\frac{\nu}{u_d D}\sqrt{\frac{2u_d^2}{gD}\frac{z}{D}}\right]^{\frac{1}{2}}$$

$$= \left[\frac{\nu}{u_d D} Fr\sqrt{2\frac{z}{D}}\right]^{\frac{1}{2}} \qquad (65)$$

Therefore, due to eq.(63) and eq.(65), the shape of a Taylor bubble is dominated by 2 dimensionless groups, namely u_{tr}/u_d and $u_d D/\nu$. If it is the case that a Taylor bubble rises with drift velocity, the former dimensionless group will be always unity. Only the latter dimensionless group (Re) is to be varied to evaluate the present model. However, Re cannot be varied unboundedly. Das and Pattanayak [6] have examined air-water flow in vertical 11 mm diameter pipes and found that the transition from bubbly to slug flow occurred at 34% void fraction, independent of liquid and gas flux velocity. Cheng *et al.* [4] have studied the bubble-to-slug transition of air-water flow with 2 different pipe sizes (150 and 28.9 mm diameter), and found that traditional slug flow did not exist in larger pipes, whereas it suddenly occurred in smaller pipes by increasing the gas flow rate at a constant liquid flow rate. Kytomaa and Brennen [8] confirmed that air-water flow in vertical 102 mm diameter columns developed from bubbly flow to churn turbulent flow rather than slug flow at approximate 44.3% void fraction, under the conditions of atmospheric pressure and low liquid flux (<0.2m/s). In contrast, Sun *et al.* [15] have found that slug flow still can occur in pipes with diameter larger than 100 mm if the volumetric flowrate in the pipe is low enough (0.011m/s). In their work, an air-water mixture is circulated in a vertical pipe, which is 112.5 mm in diameter and 12 m high to assure fully-developed conditions. Also, the information from Table 1 show that slug flow happens in pipes with diameter of 25-50 mm. So, it is conclusive that slug flow probably occurs in pipes with diameter ranging from 11 mm to 112.5 mm. In this work, the pipe diameter is, thus, selected to be 25, 50 and 100 mm to cover most of the possible pipe sizes.

The simulations consider Taylor bubbles as an unmovable object obstructing liquid flowing toward its nose. The velocity of flow at the bubble nose is drift velocity calculated by eq.(64). The boundary condition along the pipe wall is considered as a no-slip condition and governed by the wall function as stated previously. A Free-shear boundary condition is posed along the gas-liquid interface since the gas density and viscosity are much lower than the liquid density and viscosity as explained in Barnea [1]. Along the centerline of pipes, a symmetry boundary condition is posed. A periodic boundary condition is exploited between inlet and outlet plane with constant forcing mass flowrate. The constant flowrate is calculated by density, flow sectional area and flow velocity, which is corresponding to bubble drift velocity at the bubble nose. The fluid in the liquid slug is water with a density of 10^3 kg/m^3 and absolute viscosity of 10^{-3} Ns/m^2.

6. Results and Discussion

The comparison between Taylor bubble shapes, computed by 2 different models is shown in Table 2 to 4 for the cases that pipe diameters are 25, 50 and 100 mm, respectively. The boundary layer thickness (δ) on the pipe wall obviously affects the shape of the Taylor bubble to be bigger at the head of the bubble (from $0D$ to $1D$) but slender afterward. The ratio between Taylor bubble shapes ($R_{present}/R_{D\&T}$) for all cases approaches a minimum. The smaller the pipe is, the smaller the minimum is. This is previously expected since the boundary layer thickness disturbs the flow more seriously within the narrower falling film occurring in the case that the pipe diameter is small. It can be also explained by a mathematical method. As shown in eq.(62), the Taylor bubble shape is affected by 2 important parameters. One of the 2 parameters is δ/D. If we divide eq.(44) with the pipe diameter, we will get :

$$\frac{\delta}{D} = \left[\nu\sqrt{\frac{2}{g}\frac{z}{D}}\right]^{\frac{1}{2}}\left[\frac{1}{D}\right]^{\frac{3}{4}} \qquad (66)$$

Table 2: The comparison of Taylor bubble shape and pressure drop along the bubble surfaces, computed by 2 different models for 25 mm pipe.

$\left(\frac{z}{D}\right)$	$\left(\frac{R_{present}}{R_{D\&T}}\right)$	$\left(\frac{\Delta p}{p_0}\right)_{present} x100$	$\left(\frac{\Delta p}{p_0}\right)_{D\&T} x100$
0.1	1.214	-0.002	0.005
0.5	1.008	-0.013	-0.007
1	0.998	-0.035	-0.038
2	0.995	-0.140	-0.191
4	0.993	-0.690	-1.013
6	0.993	-1.843	-2.817
8	0.993	-3.682	-5.833
10	0.993	-6.272	-10.204

Table 3: The comparison of Taylor bubble shape and pressure drop along the bubbles surfaces, computed by 2 different models for 50 mm pipe.

$\left(\frac{z}{D}\right)$	$\left(\frac{R_{present}}{R_{D\&T}}\right)$	$\left(\frac{\Delta p}{p_0}\right)_{present} x100$	$\left(\frac{\Delta p}{p_0}\right)_{D\&T} x100$
0.1	1.217	0.000	0.009
0.5	1.011	-0.021	-0.007
1	1.001	-0.046	-0.041
2	0.997	-0.183	-0.224
4	0.996	-0.880	-1.165
6	0.995	-2.357	-3.204
8	0.995	-4.697	-6.550
10	0.995	-7.910	-11.293

Eq.(66) states that δ/D varies with $D^{-3/4}$. Therefore, at the same z/D, δ/D will be less if the pipe diameter is larger. This agrees very well with the simulated results shown in Table 2 to 4.

Table 4: The comparison of Taylor bubble shape and pressure drop along the bubbles surfaces, computed by 2 different models for 100 mm pipe.

$\left(\frac{z}{D}\right)$	$\left(\frac{R_{present}}{R_{D\&T}}\right)$	$\left(\frac{\Delta p}{p_0}\right)_{present} x100$	$\left(\frac{\Delta p}{p_0}\right)_{D\&T} x100$
0.1	1.219	-0.018	0.018
0.5	1.012	-0.030	-0.002
1	1.002	-0.057	-0.038
2	0.999	-0.219	-0.245
4	0.998	-1.042	-1.285
6	0.997	-2.749	-3.453
8	0.997	-5.411	-6.902
10	0.997	-8.977	-11.625

The next investigated result is the static pressure along the gas-liquid interface on the liquid side. Table 2 to 4 shows pressure drop ratios, resulted from different Taylor bubble shapes. The symbol Δp refers to $p - p_0$. As previously stated, static pressure should be constant along the interface, implying that pressure drop should be zero along the interface. Both the present model and the combination of Dumitresku & Taylor models still give pressure drops. The presence of pressure drop may be caused by wall shear, which is neglected in both models. However, we will not prove this hypothesis since it is out of the scope of this work. When concluding all 3 cases of different pipe sizes, it is found that the present model gives comparatively little pressure drop within the region of the bubble head (from $0D$ to $2D$), but comparatively larger pressure drop within the region of the bubble tail (beyond $2D$). This is consistent with the ratio between Taylor bubble shapes, because the bubble head, predicted by the present model, is larger. It induces higher increasing rates of dynamic pressure, leading to higher decreasing rates of static pressure. However, the present model seems to give better shapes of Taylor bubbles when the pressure drop is seriously considered.

Kinematic energy coefficients (α) for 3 cases of different pipe size are shown in Fig.3 to

Fig.5 as a function of position (z/D). The simulated results show that α is not unity at the bubble nose. It is because, in fact, the boundary layer starts to develop approximately $0.5D$ before the bubble nose. This can be confirmed by previous works. For example, Bugg *et al.* [3] found that beyond $D/3$, in front of the bubble noses velocity is almost undisturbed, while Polonsky *et al.* [13] and Van Hout *et al.* [17] found that the flow field is undisturbed beyond $0.66D$ and $0.5D$ in front of the bubble nose, respectively. As a the result, the boundary layer thickness at $z/D=0$ is not zero, leading to $\alpha>1$ in all simulated results. In contrast, δ calculated by eq.(44) which is forced to be zero at position $z/D=0$ to eliminate the singularity term ($cz^{-29/2}$) in eq.(43). This is the reason why $\alpha_{eq.11\&19}$, which uses δ calculated by eq.(44), shows a result equal to unity at $z/D=0$.

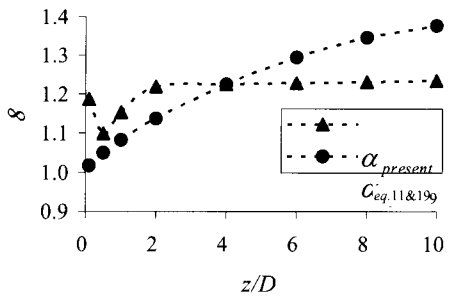

Figure 3: The comparison between α computed by the simulation with $R_{present}$ and α calculated by eq.(11) & eq.(19) in 25 mm pipe.

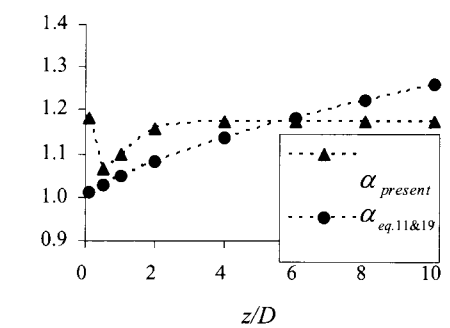

Figure 4: The comparison between α computed by the simulation with $R_{present}$ and α calculated by eq.(11) & eq.(19) in 50 mm pipe.

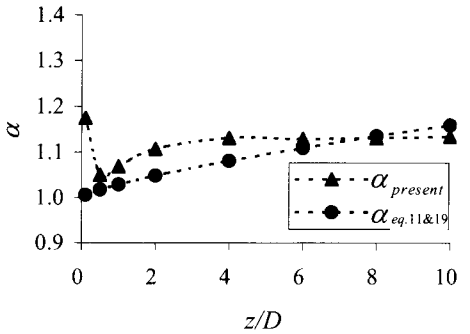

Figure 5: The comparison between α computed by the simulation with $R_{present}$ and α calculated by eq.(11) & eq.(19) in a 100 mm pipe.

Another interesting point about the curves of α is that all the curves approach a maximum value. By comparing among the results from different pipe sizes, it is found that larger pipe diameters give smaller maximum values. This can be explained by considering eq.(11) and eq.(19). In the region of the bubble tail, it is found that naturally $R\approx(D/2)$ and $\delta\rightarrow[(D/2)-R]/\chi$, in which χ is the ratio between δ and gap width $[(D/2)-R]$. Applying these assumptions into eq.(11) and eq.(19), the limit of α will be:

$$\lim_{z/D\rightarrow\infty}\alpha=\frac{\chi^2}{\chi^2-\chi-1/3}\left(1-\frac{19}{35\chi}\right) \quad (67)$$

Eq.(67) gives $\alpha=1.37$ when $\chi=1$. This is the maximum value of α since naturally δ cannot be bigger than the gap width $[(D/2)-R]$, resulting in $\chi_{\min}=1$. When D is bigger, the gap width increases, leading to higher χ, which decreases α in eq.(67).

The last interesting point about the curves of α is that, at the same pipe size, $\alpha_{present}$ reaches a higher maximum with slower rate than $\alpha_{eq.11\&19}$ does. The reason is that $\alpha_{eq.11\&19}$ is predicted under the assumption that the static pressure is constant, resulting in $\delta\propto z^{0.25}$ as shown in eq.(44). Generally, α

increases when δ is higher. But for the case of $\alpha_{present}$, it is obtained from simulation where the pressure gradient in a falling film is favorable. The favorable pressure gradient increases the momentum of flow and retards the increasing rate of δ as well as α. However, the order of magnitude of $\alpha_{present}$ and $\alpha_{eq.11\&19}$ are very close in the region of the bubble tail for all pipe sizes. This is the reason why the present model predicts quite good bubble shapes especially in the region of the bubble tail.

7. Conclusion

1. A new model for predicting the shape of Taylor bubbles by considering the effect of Kinematic energy coefficients is obtained and summarized as shown below :

$$R = \frac{D}{2}\sqrt{1-\lambda' - \frac{4}{3}\frac{\delta}{D}}$$

where $\lambda' = 2\sqrt{\psi}\cos(\phi/3)$

$$\cos\phi = \zeta/\psi^{1.5} \quad ;0^o \le \phi \le 180^o$$

$$\psi = \frac{1}{3}\gamma$$

$$\zeta = -\frac{1}{2}\left(\frac{\delta}{D}\right)\left[\frac{64}{27}\left(\frac{\delta}{D}\right)^2 + \frac{88}{105}\gamma\right]$$

$$\gamma = \left(1+\frac{2gz}{u_{tr}^2}\right)^{-1}$$

$$\delta = \left[\nu\sqrt{\frac{2z}{g}}\right]^{\frac{1}{2}}$$

2. The assumptions for deriving the new model are

2.1 The pressure along a Taylor bubble interface is constant.

2.2 The density of the mixture around a Taylor bubble is uniformly distributed.

2.3 The boundary layer thickness is much less than the pipe diameter.

2.4 The boundary layer thickness is less than the falling film gap ($\chi > 1$).

2.5 The wall shear is neglected.

3. The features of this model are

3.1 When pressure drops along a Taylor bubble interface, the new model predicts worse bubble noses but much better bubble tails in comparison to previous models.

3.2 The new model can predict the shape of whole bubbles. This is different from the previous models, which need to employ 2 (or 3) equations for predicting the shape of a whole bubble.

4. The new model can be applied in many works, for example:

4.1 Since the one-equation model gives a smoother curve of bubble shape than the two-equation model does, the shape of Taylor bubbles and the boundary layer thickness predicted by this new model will be more convenient to use for studying the flow field in thr falling film region. On the other hand, there is no need for considering the region where 2 different curves of shape merge.

4.2 The shape of Taylor bubbles predicted by the new model can be used as a reference for other experimental and computational results since it gives better bubble shapes than those predicted by previous models.

8. References

[1] Barnea, D., Effect of Bubble Shape on Pressure Drop Calculations in Vertical Slug Flow, Int. J. Multiphase Flow, Vol.16 No.1, pp.79-89, 1990.

[2] Bugg, J. D., Mack, K. and Rezkallah, K. S., A Numerical Model for Taylor Bubbles Rising Through Stagnant Liquids in Vertical Tubes, Int. J. Multiphase Flow, Vol. 24 No. 2, pp. 271-281, 1998.

[3] Bugg, J. D. and Saad, G. A., The Velocity Field Around a Taylor Bubble Rising in a Stagnant Viscous Fluid: Numerical and Experimental Results, Int. J. Multiphase Flow, Vol. 28, pp. 791-803, 2002.

[4] Cheng, H, Hills, J. H. and Azzorpardi, J., A Study of the Bubble-to-Slug Transition in Vertical Gas-Liquid Flow in Columns of Different Diameter, Int. J. Multiphase Flow, Vol. 24, No. 3, pp. 431-452, 1998.

[5] Clarke, A. and Issa, R. I., A Numerical Model of Slug Flow in Vertical Tubes, Computers & Fluids, Vol. 26, No. 4, pp. 395-415, 1997.

[6] Das, R. and Pattanayak, S., Bubble to Slug Flow Transition in Vertical Upward Two-Phase Flow through Narrow Tubes,

Chemical Engineering Science, Vol. 49, No. 13. pp. 2163-2172, 1994.

[7] Ferziger, J. H. and Peric, M., Computational Methods for Fluid Dynamics, 3rd ed., Springer-Verlag, Germany, pp. 157-308, 2002.

[8] Kytomaa, H. K. and Brennen, C. E., Small Amplitude Kinematic Wave Propagation in Two-Component Media, Int. J. Multiphase Flow, Vol. 17, No. 1, pp. 13-26, 1991.

[9] Mao, Z-S. and Dukler, A. E., Rise Velocity of a Taylor Bubble in a Train of Such Bubbles in a Flowing Liquid, Chemical Engineering Science, Vol. 40 No. 11, pp. 2158-2160, 1985.

[10] Mao, Z-S. and Dukler, A. E., The Motion of Taylor Bubbles in Vertical Tubes. I. A Numerical Simulation for the Shape and Rise Velocity of Taylor Bubbles in Stagnant and Flowing Liquid, Journal of Computational Physics, Vol. 91, pp. 132-160, 1990.

[11] Mao, Z-S. and Dukler, A. E. , The Motion of Taylor Bubbles in Vertical Tubes-II. Experimental Data and Simulations for Laminar and Turbulent Flow, Chemical Engineering Science, Vol. 46, No. 8, pp. 2055-2064, 1991.

[12] Nigmatulin, T. R. and Bonetto, F.J., Shape of Taylor Bubbles in Vertical Tubes, Int. Comm. Heat Mass Transfer, Vol. 24, No. 8, pp. 1177-1185, 1997.

[13] Polonsky, S., Shemer, L. and Barnea, D., The Relation Between the Taylor Bubble Motion and the Velocity Field Ahead of It, Int. J. Multiphase Flow, Vol. 25, pp. 957-975, 1999.

[14] Shemer, V., Hydrodynamic and statistical parameters of slug flow, International Journal of Heat and Fluid Flow, Vol. 24, pp. 334–344, 2003.

[15] Sun, B., Wang, R., Zhao, X. and Yan, D., The Mechanism for the Formation of Slug Flow in Vertical Gas–Liquid Two-Phase Flow, Solid-State Electronics, Vol. 46, pp. 2323–2329, 2002.

[16] Van Hout, R., Bernea, D., and Shemer, L., Evolution of Statistical Parameters of Gas-Liquid Slug Flow along Vertical Pipes, Int. J. Multiphase Flow, Vol. 27, pp. 1579-1602, 2001.

[16] Van Hout, R., Gullitski, A., Bernea, D., and Shemer, L., Experimental Investigation of The Velocity Field Induced by a Taylor Bubble Rising in Stagnant Water, Int. J. Multiphase Flow, Vol. 28, pp. 579-596, 2002.

[17] Van Hout, R., Bernea, D., and Shemer, L., Evolution of Hydrodynamic and Statistical Parameters of Gas-Liquid Slug Flow along Inclined Pipes, Chemical Engineering Science, Vol. 58, pp. 115 – 133, 2003.

[18] White, E. T. and Beardmore, R. H., The Velocity of Rise of Single Cylindrical Air Bubbles through Liquids Contained in Vertical Tubes, Chemical Engineering Science, Vol. 17, pp. 351-361, 1962.